China Ocean Eng., 2022, Vol. 36, No. 4, P. 658–665
DOI: https://doi.org/10.1007/s13344-022-0058-z, ISSN 0890-5487
http://www.chinaoceanengin.cn/ E-mail: coe@nhri.cn

Thermal—Fluid—Structure Coupling Analysis of Flexible Corrugated Cryogenic Hose

YANG Liang^a, LIU Miao-er^a, LIU Yun^b, LI Fang-qiu^a, FAN Jia-kun^a, LIU Fu-peng^c, LU Zhao-kuan^{d, *}, YANG Jian-ye^d, YAN Jun^{d, e}

- ^a CNOOC Gas & Power Group Co., Ltd., Beijing 100028, China
- ^b CNOOC Research Institute Co., Ltd., Beijing 100028, China
- ^c Offshore Oil Engineering Co., Ltd., Tianjin 300461, China
- ^d Ningbo Institute of Dalian University of Technology, Ningbo 315016, China
- ^e State Key Laboratory of Structural Analysis for Industrial Equipment, Department of Engineering Mechanics, International Research Center for Computational Mechanics, Dalian University of Technology, Dalian 116024, China

Received March 28, 2022; revised June 30, 2022; accepted July 18, 2022

©2022 Chinese Ocean Engineering Society and Springer-Verlag GmbH Germany, part of Springer Nature

Abstract

This work presents a numerical investigation of the thermal-fluid-structure coupling behavior of the liquid natural gas (LNG) transported in the flexible corrugated cryogenic hose. A three-dimensional model of the corrugated hose structure composed of multiple layers of different materials is established and coupled with turbulent LNG flow and heat transfer models in the commercial software ANSYS Workbench. The flow transport behavior, heat transfer across the hose layers, and structural response caused by the flow are analyzed. Parametric studies are performed to evaluate the impacts of inlet flow rate and thermal conductivity of insulation material on the temperature and structural stress of the corrugated hose. The study found that, compared with a regular operating condition, higher inlet flow velocities not only suppress the heat gain of the LNG but also lower the flow-induced structural stress. The insulation layer exhibits excellent performance in maintaining the temperature at the fluid–structure interface, showing little temperature change with respect to material thermal conductivity and ambient temperature. The simulation results may contribute to the research and design of the flexible corrugated cryogenic hoses and provide guidance for safer and more efficient field operations.

Key words: flexible corrugated cryogenic hose, LNG, computational fluid dynamics, thermal-fluid-structure coupling

Citation: Yang, L., Liu, M. E., Liu, Y., Li, F. Q., Fan, J. K., Liu, F. P., Lu, Z. K., Yang, J. Y., Yan, J., 2022. Thermal–fluid–structure coupling analysis of flexible corrugated cryogenic hose. China Ocean Eng., 36(4): 658–665, doi: https://doi.org/10.1007/s13344-022-0058-z

1 Introduction

The South China Sea has more than 100 billion tons of oil equivalent resources, among which 83% is comprised of natural gas, and 70% of the natural gas resources come from deep-water areas 500 km away from the Chinese mainland. How to economically and effectively develop natural gas resources in the deep South China Sea has become one of the primary focuses of the country's energy development (Yang et al., 2019). For deep-sea operations, the natural gas is first transported to a close-by floating LNG (FLNG), which is a floating unit responsible for storing and liquifying the natural gas before the liquid natural gas (LNG) is picked up by LNG carriers (Won et al., 2014). The traditional LNG transportation between FLNG and LNG carriers is realized by discharge arms, which requires them to align side by side

with minimal relative motions (Eide et al., 2011; Zhao et al., 2014). However, the current mooring techniques can hardly achieve that requirement under harsh environmental conditions. The introduction of flexible cryogenic corrugated hoses as a replacement for the rigid discharge arms effectively alleviates this problem. The advanced flexible corrugated hoses allow a relatively safe distance between the FLNG and LNG carrier, enhancing safety under severe sea conditions. It has found increasing applications in offshore LNG production and transportation in recent years. Currently, two main types of cryogenic LNG hoses exist: metallic corrugated cryogenic hoses and polymer material composite cryogenic hoses. The corrugated cryogenic hose is typically comprised of a metallic corrugated inner layer wrapped by insulation and tensile armor layers. It can be further divided into sus-

Foundation item: The work was financially supported by the National Natural Science Foundation of China (Grant No. U1906233), the Development Projects in Key Areas of Guangdong Province (Grant No. 2020B1111040002), and the Fundamental Research Funds for the Central Universities (Grant Nos. DUT20ZD213 and DUT20LAB308).

^{*}Corresponding author. E-mail: luzk_nbi@dlut.edu.cn

pended and floating types. This work focuses on the floating corrugated cryogenic hoses, which are widely used in LNG ship-to-ship and ship-to-shore transmission for up to several hundred meters (Bardi et al., 2011).

Owing to its long-span nature, experimental and numerical investigations have been performed on the structural performance of the flexible corrugated cryogenic hoses. Srivastava et al. (2011) assessed the strain hardening effect of the inner corrugated hose layer under the cryogenic environment by experiment and Finite Element analysis. Their results suggest that the spatial variation of strain hardening and biaxial local stresses significantly affect the fatigue response of the corrugated layer. A static strength experiment conducted by Buitrago et al. (2010) revealed that a cryogenic environment stiffens the displacement response of the structure and thus increases the fatigue life compared with the room temperature. Yang et al. (2016, 2017) proposed a multi-objective optimization approach to minimize the stiffness and stress of the flexible corrugated hose under large structural deformation.

The previous studies on the flow inside the corrugated cryogenic hoses have primarily focused on the pressure drop and friction factor, which determine the amount of energy used to transport the fluid. Pisarenco et al. (2010) numerically studied critical pressure loss inside the corrugated hoses using RANS $k-\omega$ and $k-\epsilon$ two-equation models to estimate the friction factor for the turbulent flow. Calomino et al. (2015) alternatively employed Large Eddy Simulation techniques to obtain the friction factor for large Reynolds number flows and found good agreement with the experiment. Nyarko (2012) investigated the effect of heat load on the friction factor of the laminar flow with a 2D axisymmetric corrugated hose setup and found that the friction factor monotonically decreases with stronger heat load. Jaiman et al. (2010) employed RANS and DES turbulence models to study the pressure drop and change of flow resistance during the unsteady flowing process in the corrugated hose and concluded that the depth of corrugation has a significant influence on the pressure drop. Li et al. (2018) experimentally compared the pressure drop and friction factor between slush nitrogen and subcooled liquid nitrogen and found no significant difference as long as the structure fraction in slush nitrogen is below 20%. Wang et al. (2019) assessed flow characteristics inside a flexible corrugated hose and found that backflow may occur at the fluid inlet, and cavitation may be generated near the outlet with a high Reynolds number. In terms of heat transfer performance of the corrugated hoses, studies have shown that the total heat transfer coefficient of the corrugated wall is significantly higher than that of the smooth wall due to the larger surface area (Fabbri, 2000; Naphon, 2007). Compared with a smooth wall, the corrugated structure may increase the strength of turbulence in the flow, accelerating heat exchange between the fluid and hose wall. Rising in temperature above the boiling point may vaporize the LNG, significantly increasing the pressure on the hose wall and reducing the LNG transportation efficiency. Moreover, the heat conduction of the fluid flow in the tube may cause the hose to deform due to the structural thermal expansion. As a result, transporting LNG in a corrugated cryogenic hose involves complex thermal–fluid–structure coupling mechanisms. Despite the previous assessments on the flow, structural, and heat transfer behavior of the flexible cryogenic hoses, a systematic thermal–fluid–structure coupled analysis is absent. The highlight of this work is to fill this knowledge gap with a focus on the mechanical and thermal interaction between the LNG and the flexible corrugated hose structure. The findings of this work may help to optimize the LNG transport efficiency and enhance operational safety.

The rest of this paper is organized as follows. Section 2 begins with the description of the numerical models for the thermal–fluid–structure coupling analysis. In Section 3, flow transportation velocity and pressure behaviors, temperature field, and structural response are analyzed under a regular hose operating condition. More parametric studies on the effect of inlet flow velocity and insulation material thermal conductivity on the thermal and structural response of the coupled system are carried out in Section 4, and conclusions are summarized in Section 5.

2 Numerical methods

This section introduces the numerical models for the fluid, structure, heat transfer, and their coupling. Commercial software ANSYS Workbench is employed for meshing and discretizing the numerical models. The governing equations for each model are briefly described following (ANSYS, 2020a, 2020b, 2020c). Assuming a small displacement of the corrugated wall, one-way coupling method is adopted for the coupling of mechanical field and thermal field between fluid and structure. The steady-state solutions of the flow field (e.g., velocity and pressure) and temperature field of the fluid and structure are firstly solved in the FLU-ENT module with a static fluid-structure interface. Then, the corresponding fluid pressure load and structure body temperature are imported into the Static Structural module to obtain the structural response (e.g., displacement and stress).

2.1 Cryogenic corrugated hose model

The modeled corrugated hose has a total length of 6 m, with its components configuration based on the design parameters extracted from the previous publications (Eide et al., 2011; Yang et al., 2018). A section of the hose model is shown in Fig. 1. The corrugation curvature features continuous alternating half circles with a radius of 8.25 mm. The pipe has a minimum inside diameter of D = 203 mm. With the gravitational force along the x axis being neglected, only half of the hose is simulated to save the computational efforts. From the inside to the outside, the layers are the cor-

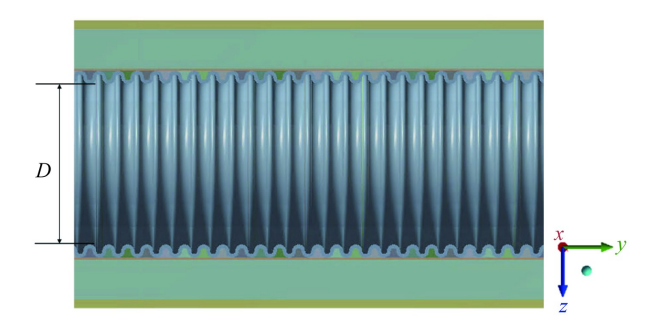


Fig. 1. A section of the modeled cryogenic corrugated hose.

rugation layer in contact with the fluid, the filling layer, the armor layer, the insulation layer, and the outer protective layer. Table 1 lists the dimensions and material properties of each hose layer used for the structural and heat transfer models.

2.2 Structural governing equations

The static structural response is solved in the Lagrangian framework with the assumption of elastic deformation (linear static structural analysis) by the differential equation:

$$\nabla \cdot \boldsymbol{\sigma} + \boldsymbol{F} = 0, \tag{1}$$

where F is the external load on the fluid–structure interface (gravitational force is neglected given the floating nature of the hose), and the stress vector, σ , can be expressed by the elastic strain, ϵ , and elastic stiffness matrix, D, as $\sigma = D\epsilon^{\rm el}$. The elastic strain with consideration of the thermal expansion effect can be written as:

$$\boldsymbol{\epsilon}^{\mathrm{el}} = \boldsymbol{\epsilon} - \boldsymbol{\epsilon}^{\mathrm{th}},\tag{2}$$

where the total strain, ϵ , and thermal expansion induced strain vector, ϵ^{th} , can be expressed as $\left[\epsilon_x \ \epsilon_y \ \epsilon_z \ \epsilon_{xy} \ \epsilon_{yz} \ \epsilon_{xz}\right]^{\text{T}}$ and $(T-T_{\text{ref}})\left[\alpha_x \ \alpha_y \ \alpha_z \ 0 \ 0 \ 0\right]^{\text{T}}$, in which T and T_{ref} are the structural temperature and the reference temperature, respectively, and α_x , α_y , and α_z are the secant coefficient of thermal expansion in each direction. Here, the materials are assumed to be isotropic, therefore $\alpha_x = \alpha_y = \alpha_z$. The structural domain is spatially discretized by hexahedral-dominant mesh with linear elements. The LNG inlet end is set as a fixed boundary, and the outlet end is designated as a free boundary. For the symmetric plane, a frictionless boundary condition is prescribed. A schematic diagram of the boundary conditions can be found in Fig. 2.

Table 1 Material properties of each layer of the cryogenic corrugated hose.

	Corrugated layer	Filling layer	Armor layer	Insulation layer	Outer protective layer
Material	ASTM 316L stainless steel	Polyurethane foam	Polyester fiber	Polyethylene foam	Rubber
Thickness (mm)	4.5	1	2	50	10
Density (kg/m ³)	8000	1050	1380	220	976
Young's modulus (MPa)	193000	200	84000	90	950
Poisson's ratio	0.3	0.43	0.36	0.3	0.38
Specific heat capacity [J·(kg·°C) ⁻¹]	460	1400	1700	1500	1700
Thermal conductivity [W/(m·K)]	25	0.085	0.2	0.025	0.15
Thermal expansion coefficient (µm/m·°C)	10	40	120	180	80

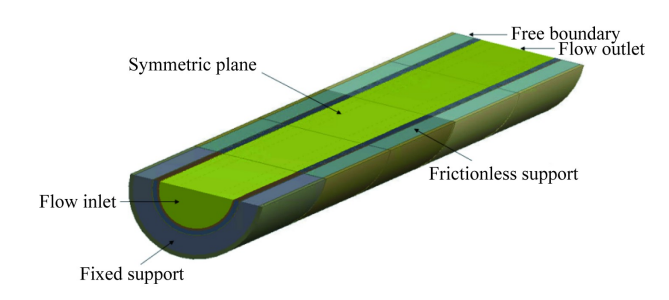


Fig. 2. Schematic diagram of boundary conditions.

2.3 Fluid governing equations

The LNG flow (material properties listed in Table 2) inside the flexible hose is considered to be incompressible and turbulent given the low flow velocity but high Reynolds number (\sim 1×10⁶). The LNG is assumed to stay in its liquid

form, relieving the computational overhead for multiphase simulation. Reynolds-averaged Navier–Stokes (RANS) $k-\epsilon$ formulation is employed to model the turbulence effect due to its robust performance for high Reynolds number flow. Steady-state continuity and momentum equations are used to describe the flow motion:

$$\nabla \cdot \boldsymbol{u} = 0; \tag{3}$$

$$\rho(\boldsymbol{u}\cdot\nabla)\boldsymbol{u} = -\nabla\left(P + \frac{2}{3}\rho k\right) + \nabla\cdot\left(\mu + \mu_{\mathrm{T}}\right)\left[\nabla\boldsymbol{u} + (\nabla\boldsymbol{u})^{\mathrm{T}}\right],\tag{4}$$

where \boldsymbol{u} is the flow velocity vector, ρ is the fluid density, P is the flow pressure, and μ is the dynamic viscosity. k is the turbulence kinetic energy and $\mu_{\rm T}$ is the eddy viscosity, both created by the Boussinesq approximation to capture the effect of turbulence fluctuation. $\mu_{\rm T}$ is calculated by k and its dissipation rate ϵ in the $k-\epsilon$ formulation as:

 Table 2
 LNG material properties

Density (kg/m ³)	Specific heat capacity $[J \cdot (kg \cdot {}^{\circ}C)^{-1}]$	Thermal conductivity [W/(m·K)]	Viscosity (kg·m ⁻¹ ·s ⁻¹)	Boiling point (°C)
414	3478	0.195	0.00010988	-162

$$\mu_{\rm T} = \rho C_{\mu} \frac{k^2}{\epsilon},\tag{5}$$

where C_{μ} is a constant coefficient. Two additional transport equations of k and ϵ for closing the fluid governing equation are omitted for brevity. The velocity–pressure coupling is realized by the SIMPLE algorithm. The enhanced wall treatment is applied to capture the viscous effect near the wall. The fluid domain is spatially discretized by hexahedral-dominant mesh with linear elements as well. The corrugation wall is set as a non-slip boundary and inflated with 5 prims layers with a expansion ratio of 1.2. The height of the first layer is configured to make y+~1. For the simulations performed in Sections 3 and 4, a velocity boundary condition is set at the hose inlet and a zero-pressure boundary condition is prescribed at the outlet (see Fig. 2).

2.3.1 Fluid solver validation

Owing to the absence of experimental data, the fluid solver is validated by an experiment performed by Calomino et al. (2015) on a 0.812 m long corrugated pipe with a sinusoidal corrugation structure. Half of the fluid domain with a symmetric plane is built, as shown in Fig. 3. A periodic boundary condition is imposed at both ends of the pipe to represent a fully-developed flow condition. By imposing a volumetric flow rate of Q = 10.2 L/s, the friction factor is calculated by the pressure head loss H_f and bulk flow velocity U using the Darcy–Weisbach function:

$$H_f = f \frac{L}{D} \frac{U^2}{2g},\tag{6}$$

where L is the pipe length and D is the minimum pipe diameter, which is 0.171 m in this case.

The current fluid solver yields a friction factor of 0.0880, which has a 4.76% deviation from the experimental result (0.0840). The small difference suggests the overall satisfactory performance of the solver.

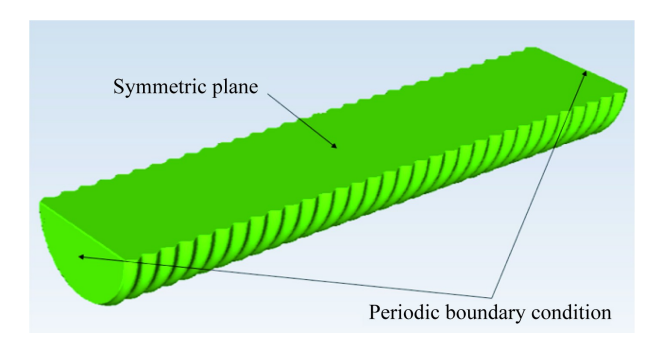


Fig. 3. Fluid domain for solver validation.

2.4 Energy governing equations

Since the temperature difference between the environment and LNG inside the hose, heat conduction is unavoidable despite the presence of the thermal insulation layer. The motion of LNG also induces heat convection within the liq-

uid. These heat transfer effects can be modeled by the energy equation of the fluid and structure. In the fluid region, the energy governing equation has the following form:

$$\nabla \cdot [\boldsymbol{u} (\rho E + p)] = \nabla \cdot \left[k_{\text{eff}} \nabla T - \sum_{j} h_{j} \boldsymbol{J}_{j} + (\bar{\tau}_{\text{eff}} \cdot \boldsymbol{u}) \right] + S_{\text{h}}, \quad (7)$$

where u is the flow velocity, E is the energy, h_j and J_j are the sensible enthalpy and diffusion flux of species j, and $\bar{\tau}_{\rm eff}$ is the effective viscosity. The term on the left-hand side (LHS) of Eq. (7) represents energy transfer due to convective heat transfer caused by fluid motion. The first term on the right-hand side (RHS) of Eq. (7) denotes energy transfer due to heat conduction (in the static fluid). Effective conductivity $k_{\rm eff}$ is the combination of the fluid conductivity, k, and turbulent thermal conductivity $k_{\rm t}$. The second and third terms on the RHS stand for the energy transfer caused by species diffusion (absent due to single phase) and viscous dissipation. $S_{\rm h}$ represents the volumetric heat source, which is not considered in the current modeling. On the other hand, the energy equation of the structure region takes a simpler form as no turbulence or species diffusion occurs:

$$\nabla \cdot (\mathbf{v}\rho h) = \nabla \cdot (k\nabla T),\tag{8}$$

which regulates the equilibrium between the energy transfer caused by the heat convection (LHS) and heat conduction (RHS). v represents structural velocity. Sensible enthalpy h can be calculated by the integral of specific heat capacity from the reference temperature to the current temperature. A constant temperature boundary condition is prescribed on the external hose surface to consider the surrounding environment. The rest of the boundaries is set to be heat flux free except for the inlet where the initial temperature of the LNG is applied.

3 Analysis of flow, thermal and structural behavior

This section reports simulation results of the flow transportation behavior, temperature field, and structural response with the inlet LNG flow velocity, $v_{\rm in} = 6 \, {\rm m/s}$ ($Re = 4.59 \times 10^6$), which is a regular working condition for LNG transportation. The temperature of the inlet LNG flow and the external hose surface are set to be $-165^{\circ}{\rm C}$ and $25^{\circ}{\rm C}$, respectively.

3.1 Flow velocity and pressure field

The flow velocity profile on the symmetric plane (Fig. 4) reveals a change of flow pattern at the flow entrance from the inlet to the outlet. In the flow entry region, expanding boundary layer due to the viscous force from the wall pushes the flow to the center of the hose, where the largest velocity is present. The velocity magnitude slightly drops after reaching its maximum value in the first half of the hose, which is likely caused by the loss of pressure head due to the enhanced turbulence by the corrugation. This is supported by the contour of turbulence kinetic energy (Fig. 5), which

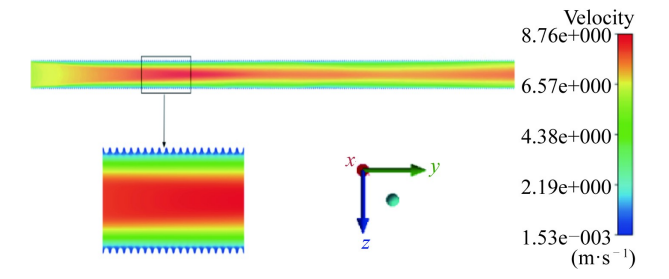


Fig. 4. Velocity magnitude contour plot of the fluid symmetric plane.

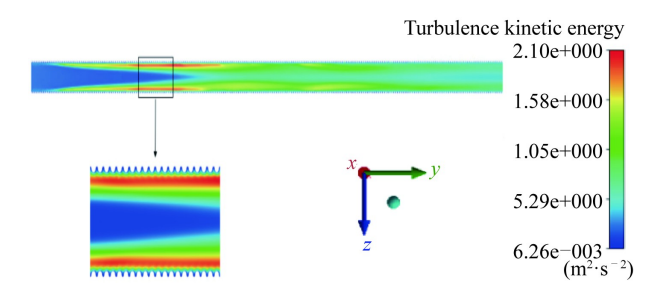


Fig. 5. Turbulence kinetic energy contour plot of the fluid symmetric plane.

suggests the degree of turbulence grows in the flow entry region before reaching its peak and stays at a relatively uniform level for the rest of the hose length. It is interesting to note that both the flow velocity and turbulence level are the smallest at the trough of the corrugated wall. The bluff body shaped corrugations also reduce the flow pressure behind it, which induces negative pressure near the hose outlet where the pressure head becomes low, as shown in Fig. 6. This indicates a possibility of flow cavitation and pipe erosion

3.2 Fluid and structure temperature field

At the steady state, the temperature at the fluid–structure interface is barely changed, with an average of -164.99° C. It can be seen from the temperature contour plot (Fig. 7) that most of the heat conduction takes place in the insulation layer (the second outermost layer), which effectively maintains the LNG inside the hose at a constant temperature below the boiling point. The flow temperature also changes little along the hose length, with an almost indiscernible increase in temperature downstream due to the heat generated by wall friction (Fig. 8).

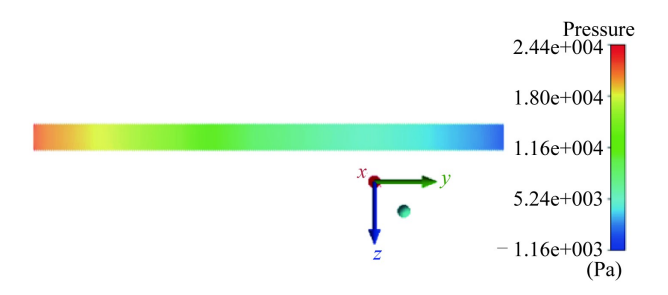


Fig. 6. Pressure contour plot of the fluid symmetric plane.

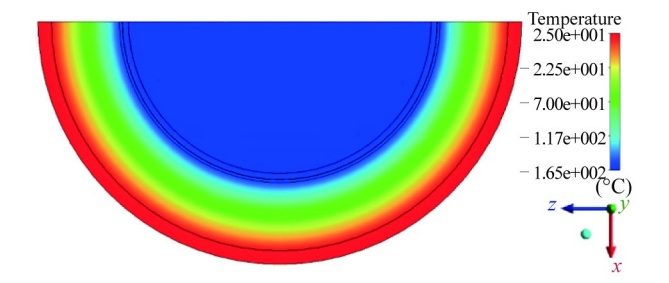


Fig. 7. Temperature contour plot of a transverse cross-section at the middle of the base

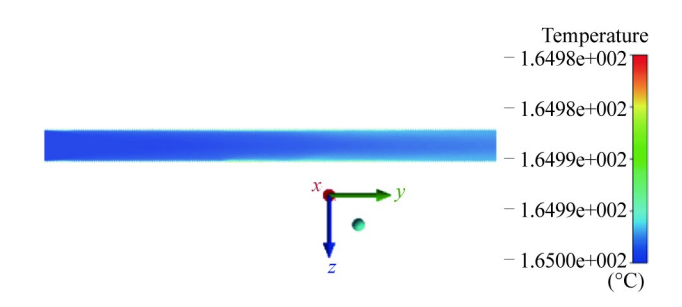


Fig. 8. Temperature contour plot of the fluid symmetric plane.

3.3 Hose structural response

Besides the external load from the marine environment, internal loads induced by the flow inside the corrugated hose also significantly affect the structural response. Since the external load depends on the specific operating environment, this work mainly focuses on the structural response caused by the internal LNG flow. With the inlet fixed and outlet free boundary condition, the largest structural displacement along the hose longitudinal direction (y direction) is found at the outlet (Fig. 9). The positive displacement near the inlet is caused by the pressure load of the flow, while the negative displacement in the second half of the hose, where the pressure load becomes much smaller, can be attributed to the larger structural contraction caused by the low-temperature fluid. Along the transverse direction (z direction), the structural displacement is mostly induced by the structural contraction (i.e., negative thermal expansion) with a magnitude much smaller than that along the longitudinal direction (Fig. 10). Overall, the small structural displacement justifies the one-way fluid-structure interaction approach used in this work.

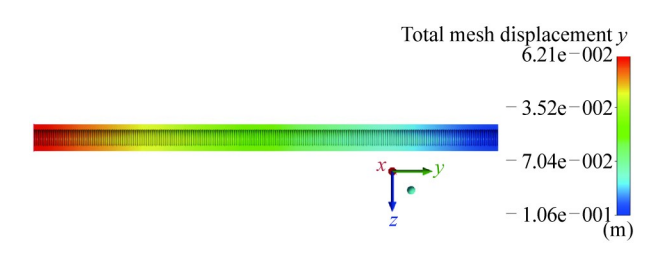


Fig. 9. Structural displacement contour plot along the longitudinal direction.

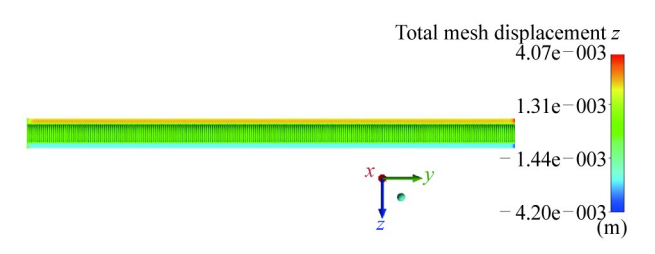


Fig. 10. Structural displacement contour plot along the transverse direction.

4 Parametric studies and discussion

In this section, parametric studies are performed by the coupled thermal—fluid—structure model proposed in Section 2. Specifically, the effects of inlet LNG flow velocity on the fluid—structure interface temperature and structural response and the thermal conductivity of the insulation layer on the structure temperature distribution are assessed.

4.1 Effects of flow velocity on temperature distribution

As mentioned in Section 1, the state of LNG inside the hose is sensitive to temperature change. It is therefore critical to understand the effects of hose operating conditions on the thermal behavior of the fluid. Fig. 11 shows the relationship with the inlet flow velocity, $v_{\rm in}$, (sampled at 2, 4, 6, 8, 10 m/s), which is most likely to be adjusted during field operations, and the average temperature at fluid–structure interface. In spite of a small variation, a smaller $v_{\rm in}$ does permit more heat gain of the liquid compared with a larger velocity. This could be explained by the prolonged time for heat conduction at the fluid–structure interface when the flow is slow. Nevertheless, it is safe to conclude that the temperature of LNG is not sensitive to the flow velocity at the order of magnitude of the regular working condition (i.e., $v_{\rm in}$ =6 m/s).

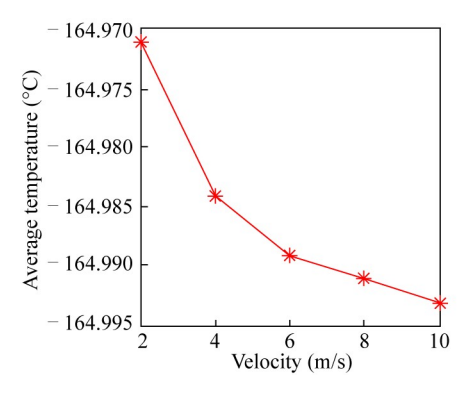


Fig. 11. Average temperature at fluid-structure interface with different inlet flow velocities.

4.2 Effects of flow velocity on structural stress response

For a smoothed wall, the flow load on the structure is mainly caused by the frictional shear stress, which is proportional to the gradient of velocity in the direction perpendicular to the flow. Given the non-slip boundary (i.e., zero velocity at wall surface) and flow parallel to the wall, a larger load can be expected with a larger flow velocity. However, this may not hold true for the corrugated walls as the flow is no longer parallel to the wall surface. By plotting the inlet velocities sampled in Section 4.1 against the average von Mises stress of the hose (Fig. 12), it can be found that structural stress does not monotonically increase with the inlet flow velocity. The structural stress peaks at $v_{in} = 6 \text{ m/s}$ then decreases as the inlet velocity becomes larger. This might be explained by the fact that less flow enters the trough region of the corrugation with larger flow velocities, therefore exerting less frictional load on the wall. On the other hand, smaller flow velocities fail to generate comparable shear stress due to smaller parallel velocity component to the wall. In general, the results suggest that operating the flow at the velocity larger than the regular inlet velocity $(v_{\rm in} = 6 \text{ m/s})$ can reduce structural load and improve transportation efficiency (i.e., less stress from the wall as well). With the better thermal performance observed in Section 4.1, an inlet flow velocity larger than the regular value is recommended in field operations.

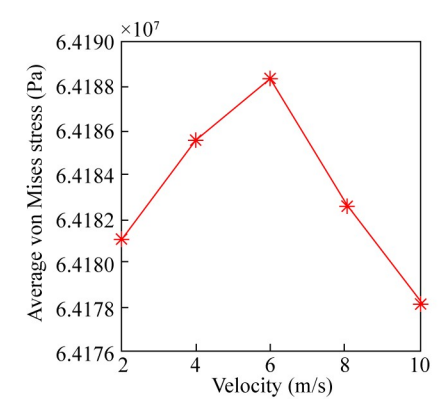


Fig. 12. Average structural von Mises stress with different inlet flow velocities.

4.3 Effects of thermal conductivity of insulation layer on temperature distribution

Since the heat exchange between the LNG and the environment mainly occurs in the insulation layer, the thermal conductivity of its material is an essential factor in the insulation performance of the cryogenic hose. In addition to the thermal conductivity of 0.025 W/($m \cdot K$) assessed in the previous simulations, five conductivity values of 0.015, 0.035, 0.045, 0.055, and 0.065 W/(m·K) are evaluated, covering the range of common insulation materials. The resultant average temperature of the fluid-structure interface plotted in Fig. 13 suggests an almost linear relationship between the thermal conductivity and interface temperature. The small variation indicates an excellent thermal performance of the insulation layer. Fig. 14 presents the temperature distribution along the transverse direction on the symmetric plane (sampled at the middle of the hose as shown in Fig. 15) for each thermal conductivity, with the location of the fluid-structure

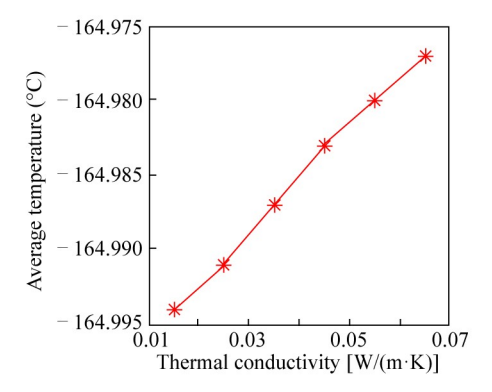


Fig. 13. Average temperature at fluid-structure interface with different thermal conductivities.

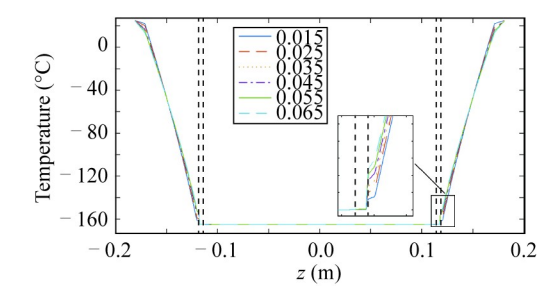


Fig. 14. Transverse temperature distribution on the symmetric plane for each thermal conductivity.

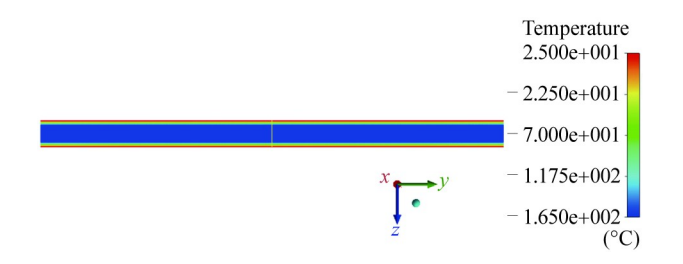


Fig. 15. Illustration of the temperature sample line.

interface and insulation layer inner surface marked by dotted lines. The temperature distribution exhibits a sharp gradient across the inner surface of the insulation layer (outer dotted line) due to a drastically different thermal conductivity between the insulation layer and the armor layer adjacent to it. All the assessed insulation materials can effectively lower the temperature at the inner surface of insulation layer within [-165°C, -155°C], ensuring a temperature low enough at the fluid–structure interface (inner dotted line). However, it is worth mentioning that a small change of temperature could still vaporize the cryogenic liquid inside the hose if the initial temperature is close to the boiling point. Therefore, discretion should be practiced in the selection of insulation materials.

4.4 Effects of ambient temperature on thermal and structural response

In field application, the cryogenic hose may operate under drastically different ambient temperatures. To assess its thermal and mechanical performance in such different environment, temperatures from 15° C to 35° C with an interval of 5° C are imposed on the outer surface of the hose, and the average temperature at the fluid-structure interface and average von Mises stress of the structure are obtained. The thermal conductivity and flow velocity are set to be 0.025 W/(m·K) and 6 m/s, respectively.

The results plotted in Fig. 16 suggest that the interface temperature is insensitive, albeit proportional to the ambient temperature, with only 0.003°C variation. The structural stress, by contrast, is inversely proportional to the ambient temperature due to the fact that higher boundary temperature mitigates the stress induced by the thermal expansion of the structural layers. Therefore, the cryogenic corrugated hose design should take the lowest possible ambient temperature into consideration.

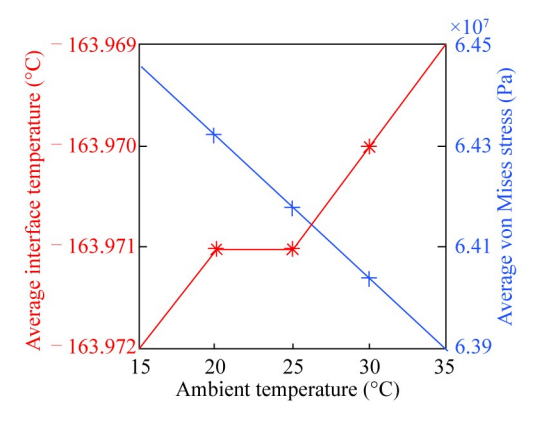


Fig. 16. Relationship between ambient temperature and average fluid–structure interface temperature and average structural von Mises stress.

5 Conclusions

This paper presented a thorough assessment of the thermal–fluid–structure coupled performance of the flexible cryogenic corrugated hose. Computational fluid and solid mechanics, along with heat transfer simulations, were carried out in ANSYS Workbench to assess the mechanical and thermal interaction between the LNG flow and the flexible corrugated hose structure.

It was found that the corrugated structure induces negative pressure around the hose outlet, potentially causing fluid cavitation. The insulation material currently used in the hose design is shown to properly block the heat conduction from the environment and maintain the temperature of LNG well below the boiling point. Furthermore, parametric studies on the inlet flow velocity suggested that the temperature at the fluid–structure interface could be elevated by a slow-moving flow due to an increased duration of heat conduction. The results also revealed a nonlinear relationship between the flow velocity and the structural stress response. Unlike the smooth hose, in which case higher stress is experienced with a larger flow velocity, the corrugated hose structural

stress drops after the flow velocity rises above a certain threshold. This is because less flow enters the trough region of the corrugated profile at a larger flow velocity, thus reducing the total frictional surface stress. Parametric assessment of the thermal conductivity of the insulation layer showed no significant change in the steady-state temperature at the fluid–structure interface in spite of a linear relationship between the thermal conductivity and the temperature, which suggests excellent performance of the common insulation materials. This is further demonstrated by the insensitive interface temperature to the ambient temperature. However, the lower ambient temperature does allow larger structural stress, which should be cautioned during the design process.

The findings of this paper may have an important contribution to the R&D and field operations of flexible corrugated cryogenic hoses. In future investigations, more experiments should be carried out to validate the current coupling framework. In addition, liquid-vapor two-phase flow could be incorporated to account for the potential LNG vaporization.

References

- ANSYS, 2020a. ANSYS FLUENT Theory Guide 2020 R1, ANSYS. ANSYS, 2020b. ANSYS Workbench User's Guide 2020 R1, ANSYS. ANSYS, 2020c. Theory Reference 2020 R1, ANSYS.
- Bardi, F.C., Tang, H., Kulkarni, M. and Yin, X.L., 2011. Structural analysis of cryogenic flexible hose, *Proceedings of the ASME 2011* 30th International Conference on Ocean, Offshore and Arctic Engineering, ASME, Rotterdam, The Netherlands, pp. 593–606.
- Buitrago, J., Slocum, S.T., Hudak Jr, S.J. and Long, R., 2010. Cryogenic structural performance of corrugated pipe, *Proceedings of the ASME 2010 29th International Conference on Ocean, Offshore and Arctic Engineering*, ASME, Shanghai, 331–342.
- Calomino, F., Tafarojnoruz, A., De Marchis, M., Gaudio, R. and Napoli, E., 2015. Experimental and numerical study on the flow field and friction factor in a pressurized corrugated pipe, *Journal of Hydraulic Engineering*, 141(11), 04015027.
- Eide, J., Bernson, M., Haakonsen, R. and Frohne, C., 2011. Challenges and solutions in the development of a flexible cryogenic pipe for offshore LNG transfer, *Paper presented at the OTC Brasil*, Offshore Technology Conference, Rio de Janeiro, Brazil.
- Fabbri, G., 2000. Heat transfer optimization in corrugated wall channels, *International Journal of Heat and Mass Transfer*, 43(23), 4299–4310.
- Jaiman, R.K., Oakley Jr, O.H. and Adkins, J.D., 2010. CFD modeling

- of corrugated flexible pipe, *Proceedings of the ASME 2010 29th International Conference on Ocean, Offshore and Arctic Engineering*, ASME, Shanghai.
- Li, Y.J., Wu, S.Q. and Jin, T., 2018. Experimental investigation on pressure drop and friction factor of slush nitrogen turbulent flow in helically corrugated pipes, *Cryogenics*, 94, 56–61.
- Naphon, P., 2007. Heat transfer characteristics and pressure drop in channel with V corrugated upper and lower plates, *Energy Conversion* and *Management*, 48(5), 1516–1524.
- Nyarko, I.P.R., 2012. Heat load and its effects on fluid friction factor in corrugated pipes, *American Journal of Scientific and Industrial Research*, 3(4), 241–251.
- Pisarenco, M., Van Der Linden, B., Tijsseling, A., Ory, E. and Dam, J., 2010. Friction factor estimation for turbulent flows in corrugated pipes with rough walls, *Journal of Offshore Mechanics and Arctic Engineering*, 133(1), 011101.
- Srivastava, V., Buitrago, J. and Slocum, S.T., 2011. Stress analysis of a cryogenic corrugated pipe, *Proceedings of the ASME 2011 30th International Conference on Ocean, Offshore and Arctic Engineering*, ASME, Rotterdam, The Netherlands, pp. 411–421.
- Wang, H.Y., Liu, M.E., Yang, L., Chen, J., Xu, J.W. and Fan, J.K., 2019. Simulation and analysis of flow characteristics for the fluid in low-temperature LNG corrugated flexible pipe, *China Offshore Oil* and Gas, 31(5), 183–189. (in Chinese)
- Won, W.Y., Lee, S.K., Choi, K. and Kwon, Y., 2014. Current trends for the floating liquefied natural Gas (FLNG) technologies, *Korean Journal of Chemical Engineering*, 31(5), 732–743.
- Yang, L., Liu, M.E., Liu, Y., Li, X.X., Fan, J.K., Xu, J.W., Gai, X.G. and Liu, F.P., 2019. Analysis on current situation and application prospect of FLNG cryogenic hose technology, *Ocean Engineering Equipment and Technology*, 6(6), 810–818. (in Chinese)
- Yang, L., Liu, M.E., Liu, Y. and Xu, J.W., 2018. Progress of the research on unloading system for LNG floating production storage and offloading unit, *Naval Architecture and Ocean Engineering*, 34(3), 8–14. (in Chinese)
- Yang, Z.X., Yan, J., Chen, J.L., Lu, Q.Z. and Yue, Q.J., 2017. Multiobjective shape optimization design for liquefied natural gas cryogenic helical corrugated steel pipe, *Journal of Offshore Mechanics* and Arctic Engineering, 139(5), 051703.
- Yang, Z.X., Yan, J., Lu, Q.Z., Chen, J.L., Wu, S.H., Wang, L.D. and Yue, Q.J., 2016. Multi-objective shape optimization design for LNG cryogenic helical corrugated steel pipe, *Proceedings of the ASME 2016 35th International Conference on Ocean, Offshore and Arctic Engineering*, ASME, Busan, South Korea, pp. 1–12.
- Zhao, W.H., Yang, J.M., Hu, Z.Q. and Tao, L.B., 2014. Prediction of hydrodynamic performance of an FLNG system in side-by-side offloading operation, *Journal of Fluids and Structures*, 46, 89–110.